Macromolecules

Article

pubs.acs.org/Macromolecules

Systematic Variation of Fluorinated Diketopyrrolopyrrole Low Bandgap Conjugated Polymers: Synthesis by Direct Arylation Polymerization and Characterization and Performance in Organic Photovoltaics and Organic Field-Effect Transistors

Patrick Homyak,[†,§] Yao Liu,[†,§] Feng Liu,[‡] Thomas P. Russel,[*,†,§] and E. Bryan Coughlin[*,†,§]

[†]Department of Polymer Science & Engineering, University of Massachusetts Conte Center for Polymer Research, 120 Governors Drive, Amherst, Massachusetts 01003, United States

[‡]Materials Science Division, Lawrence Berkeley National Laboratory, 1 Cyclotron Road, Berkeley, California 94720, United States

[§]Energy Frontier Research Center PHaSE, University of Massachusetts, Amherst Massachusetts 01003, United States

Supporting Information

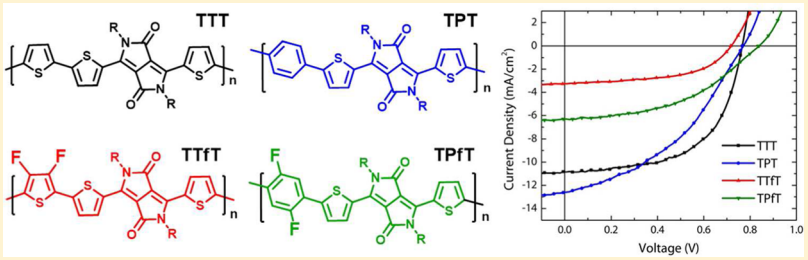

ABSTRACT: The synthesis of four different diketopyrrolopyrrole (DPP) low bandgap polymers by direct arylation polymerization (DArP) is reported. These materials were designed for use in organic photovoltaic (OPV) and organic field-effect transistor (OFET) devices. While the DPP conjugated unit was held constant for each of the materials, the alternating unit of the copolymer was varied from thiophene (TTT), to phenyl (TPT), to 3,4-difluorothiophene (TTfT), to 2,5-difluorophenyl (TPfT) creating a series of DPP materials that can be used to study structure−property-performance relationships. Molecular weights (M_w) of 17−110 kg/mol were achieved by DArP and the resulting polymers displayed excellent optical and electrical properties, comparable to previous reports of similar materials synthesized by Stille or Suzuki polycondensation. The fluorinated TTfT and TPfT materials had similar absorption profiles, but exhibited reduced E_{homo} levels (by 0.1−0.2 eV) relative to TTT and TPT, which is due to the incorporation of the highly electron withdrawing fluorine atoms. OPVs fabricated with the TTT and TPT materials reached average power conversion efficiencies of nearly 4%. Additionally, OFET hole mobilities on the order of 10^{-2} cm^2 V^{-1} s^{-1} were achieved and the fluorine substituted TTfT and TPfT materials exhibited a 2- to 3-fold improvement in hole mobility versus their nonfluorinated analogues.

1.0. INTRODUCTION

Materials containing diketopyrrolopyrrole (DPP) units in the polymer backbone have been extremely popular for use in organic electronic devices such as organic field-effect transistors (OFETs) and organic photovoltaics (OPVs).[1−3] Some recent highlights have demonstrated that DPP-based alternating copolymers can produce OPV devices with efficiencies of ∼8% in a single junction configuration, or even higher in tandem or triple junction device configurations.[4−6] The DPP units are used typically as electron deficient "acceptor" type building blocks, and when alternated with a variety of electron rich "donor" units, low bandgap "donor−acceptor" type conjugated polymers can be synthesized with relative ease. DPP based materials were initially investigated to be used as pigments[7] but have been more recently popularized for use in organic electronics applications. Over the past few years, a plethora of new DPP-containing polymeric structures have been synthesized by combining DPP with a variety of different accepting blocks, by altering the heteroatoms on DPP, by changing the identity of the solubilizing alkyl groups, or by altering the polymer architecture (i.e., linear, graft, star).

DPP based materials have relatively simple, synthetically achievable polymer structures compared to most low bandgap type polymers and have been shown to have many favorable, sought-after properties of materials for OPV active layers, such as low bandgaps (i.e., strong absorption over the majority of the visible spectrum), properly aligned molecular orbital energy levels, and reasonable solubility in organic solvents. Two examples of particular importance for this work, PDPPTTT and PDPPTPT, displayed efficiencies of 4−5% in initial reports,

Received: June 11, 2015
Revised: August 21, 2015
Published: September 17, 2015

DOI: 10.1021/acs.macromol.5b01275
Macromolecules 2015, 48, 6978−6986

Scheme 1. Synthesis of TTT, TPT, TTfT, and TPfT by Direct Arylation Polymerization (DArP)[a]

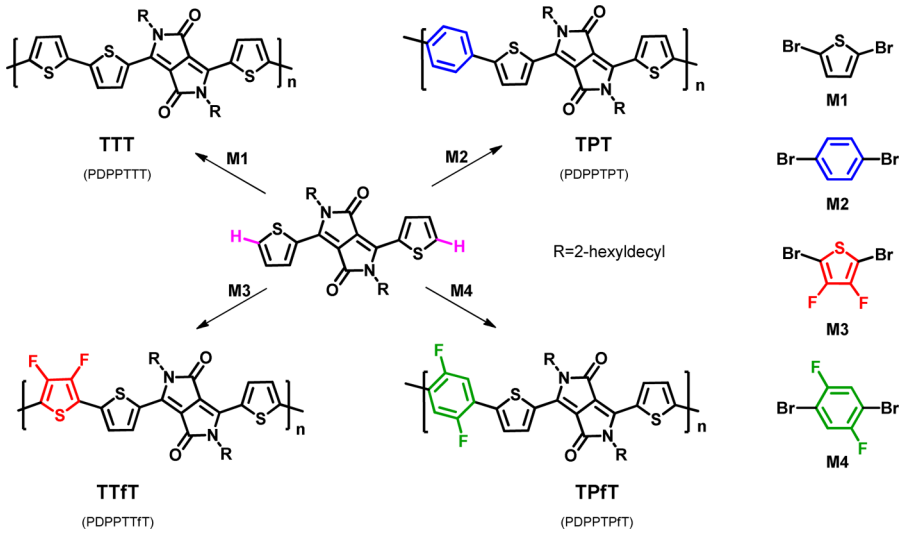

[a]DArP conditions: DPP (1 equiv), M1-M4 (1 equiv), $Pd_2dba_3{\cdot}CHCl_3$ (3 mol %), P(*o*-MePh)$_3$ (12 mol %), PivOH (1 equiv), and Cs_2CO_3 (3 equiv) in toluene:DMF (10:1 v/v, 0.05 M), heated at 115 °C for 20 h.

with higher molecular weight materials (M_p > 100 kg mol^{-1}) attaining efficiencies of ∼7% in later examples.[5,8,9] In these examples materials were synthesized by optimized Stille and Suzuki coupling polycondensation methods.

In contrast to most previous synthetic reports of DPP-based polymers, we sought to utilize an alternative direct arylation polymerization (DArP) method to demonstrate the capability of this synthetic method for producing high quality conjugated materials. DArP has recently been employed as an alternate synthetic method due to the following advantages (i) fewer overall synthetic steps, (ii) greater ease of monomer purification, and (iii) elimination of harmful toxic byproducts associated with other coupling chemistries. In contrast to other coupling chemistries, DArP can create new aromatic C−C linkages from aryl halides and activated aromatic C−H bonds. Many reports have detailed the use of DArP methods for the synthesis of conjugated polymers with a large variety of small molecule building blocks.[10−13] A few recent reports have studied the use of DArP as a method for producing small molecule and polymeric DPP based materials for OPV and OFET applications.[14−21]

In this report four DPP based materials will be discussed, PDPPTTT and PDPPTPT and their difluorinated derivatives PDPPTTfT and PDPPTPfT, respectively. For brevity, and since they all share the same DPP unit in the polymer structure, PDPPTTT, PDPPTPT, PDPPTTfT, and PDPPTPfT will here in be referred to as TTT, TPT, TTfT, and TPfT, respectively. Conjugated polymers with fluorine substituents have been of great interest as they have been shown in several instances to lead to improved OPV device performance through, in particular, improved V_{oc} over their nonfluorinated counterparts.[22−29] Although as we and others have also noticed, fluorination of conjugated polymers can complicate the morphology of the bulk heterojunction active layer and the electronic properties and do not guarantee better performance relative to non fluorinated materials.[30−33] Nonetheless, it is important to investigate new examples of conjugated fluorinated materials to understand the implications of fluorine substitution on polymer properties.

Here we describe the synthesis of four DPP-based polymers (TTT, TPT, TTfT, and TPfT) by DArP methods, the properties of these materials, and their performance in OPV and OFET applications. The properties of these polymers synthesized by DArP will be compared to those previously synthesized by the Stille or Suzuki coupling methods.[8,9,34,35] In this way the capability of DArP methods to produce high molecular weight, high quality DPP-based materials is demonstrated. This is the first example of the synthesis of each of these materials by DArP. The impact of fluorination on the polymer crystallinity, bulk heterojunction morphology, and therefore, the V_{oc} and device efficiency is discussed. The performance of these materials in OFETs and their charge transport properties as a function of polymer structure are also described.

2.0. RESULTS AND DISCUSSION

The monomers used in this study were either prepared as reported, as in the case of the dithienyldiketopyrrolopyrrole[36] block and 2,5-dibromo-3,4-difluorothiophene (**M3**),[37] or purchased commercially. 2-hexyldecyl solubilizing alkyl chains were chosen for the DPP block to afford reasonable polymer solubility. The polymers, TTT, TPT, TTfT, and TPfT, were then prepared using an optimized set of DArP conditions as shown in Scheme 1. Previously we showed that similar reported conditions could effectively polymerize thieno[3,4-*b*]thiophene and dibromobenzodithiophene using a slightly higher catalyst loading in THF.[38,39] However, for these DPP materials, it was found that these conditions were unable to form high molecular weight polymers in significant yield. This is more than likely due to differences in the reactivity of the chosen monomers and the subsequent solubility of the growing polymer chains. Recently, the toluene:DMF solvent system was shown to be a suitable for the formation of very high molecular weight DPP materials via traditional coupling methods.[5] Additionally, toluene and polar aprotic solvents have also been shown to be reasonable solvents for DArP with DPP-type materials.[14,15,19,20] Thus, by switching to the toluene:DMF solvent system in combination with higher reaction temperatures and

DOI: 10.1021/acs.macromol.5b01275
Macromolecules 2015, 48, 6978−6986

longer reaction times, it was found that higher molecular weight polymers could be achieved.

DArP under these conditions formed the desired polymers in reasonable yields as described in Table 1. Moderate yields were

Table 1. Molecular Weights of Polymers

	yield[a] [%]	M_p[b] [kg/mol]	M_n[b] [kg/mol]	M_w[b] [kg/mol]	$Đ$
TTT	45	46.4	29.0	110.9	3.8
TPT	29	15.5	13.5	24.2	1.8
TTfT	25	10.9	10.2	17.2	1.7
TPfT	35	13.2	10.3	19.3	1.9

[a]Calculated using $CHCl_3$ soluble portion. [b]Determined from GPC in 1,2,4-trichlorobenzene at 135 °C, using polystyrene standards.

observed due to the presence of some insoluble material and the removal of low molecular weight oligomeric residues via Soxhlet extraction. Insoluble portions can be the result of either very high molecular weight residues or cross-linked materials forming at high reaction conversion, as has been noticed in other examples of DArP.[21] The exact nature of the insoluble materials is difficult to characterize. However, it has been shown that their formation can be inhibited through careful optimization of reaction time.[21] Overall, the extracted materials were found to be reasonably soluble in a variety of chlorinated solvents. Determination of the molecular weights of the resulting polymers by GPC was difficult due to the strong tendencies of these materials to aggregate, even in moderately good solvents at elevated temperatures. This is typical for conjugated polymers with high degrees of crystallinity. The GPC molecular weight measurements were strongly dependent on the concentration of the polymer sample, as shown in the Supporting Information (Table S1). This aggregation effect and its relation to observed molecular weight has been noted previously for other DPP materials as a function of concentration and solution temperature.[9,40] It is also known that the solvent, column temperature, and the concentration of the sample influence the measured polymer molecular weight as measured by GPC (i.e., retention time, radius of gyration R_g). For consistency with existing literature, we report the molecular weights of these materials at a concentration of 1 mg/mL, at 135 °C in 1,2,4-trichlorobenzene.

Number-average molecular weights (M_n) greater than 10 kg/mol were achieved for each of the materials, with weight-average molecular weights (M_w) ranging from ~20 kg/mol to as high as 110 kg/mol for TTT. The lower molecular weights for TTfT and TPfT are likely a result of reduced solubility in the reaction solvent. It is likely that further optimization of reaction time and temperature for each pair of monomers could lead to even higher molecular weight materials in greater yields, as shown in other examples with DArP.[21] NMR and MALDI–TOF mass spectrometry were used to verify the structure of the polymers.

^1H and ^{19}F NMR spectra for each of the materials can be found in the Supporting Information (Figures S9–S16). Interpretation of conjugated polymer structures is often difficult by NMR, again due to strong intermolecular interactions between polymer chains. In this case it is difficult to exactly identify each of the proton resonances and fluorine signatures via NMR and so MALDI–TOF mass spectrometry was used as an additional tool for structure verification. As shown in the Supporting Information (Figures S1–s8), the full spectra for each of the polymers confirm that significant molecular weight materials were formed. Since MALDI–TOF spectra are heavily dependent on sample preparation, matrix and instrument settings, we do not assume that these spectra fully illustrate the entire molecular weight range but they do confirm that high molecular weight materials of an alternating polymer structure are formed. The inset spectra for each polymer are labeled to indicate the presence of the expected polymer repeat unit weights (H/H terminated) plus or minus an additional unit, absolutely confirming that the desired polymer structures were achieved. Additional lower intensity peaks in the spectra can be observed due to the loss of alkyl chain fragments, as has been demonstrated in MALDI–TOF analysis of P3HT,[41] or to an even lesser extent due to homocouplings, as evidenced by UV–vis absorption below.

The optical absorption of the polymers, both in solution and as films (Figure 1), closely resemble those measured previously by Janssen et al. for TTT and TPT materials.[8,9] TPT exhibits a blue-shifted absorbance versus TTT, which was also noticed in previous reports of these same materials synthesized by Stille and Suzuki coupling.[5] All materials have broad absorption over the majority of the visible spectrum with optical bandgaps (E_g) around 1.4–1.5 eV. TPfT displays blue-shifted absorbance compared to TTfT, which is well aligned with the shift noticed in TPT versus TTT. The fluorinated materials TTfT and TPfT display similar absorption profiles compared to TTT and TPT, respectively. This is expected, since the addition of fluorine

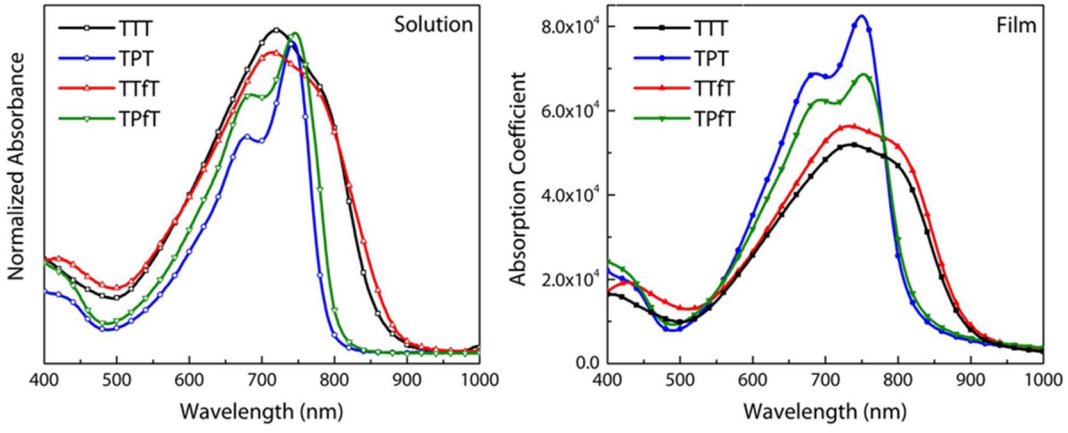

Figure 1. UV–vis absorption of dilute polymer solutions in $CHCl_3$ (left) and thin polymer films (right).

DOI: 10.1021/acs.macromol.5b01275
Macromolecules 2015, 48, 6978–6986

substituents, in most cases, lower the E_{HOMO} and E_{LUMO} levels equally, resulting in little change in the absorption profile.

It was recently noted that low-energy (i.e., red-shifted) shoulders in the absorption profile can be a signature of homocouplings present along the polymer backbone in PDPPTPT materials, due to changes in the electronic nature of the D−A polymer backbone.[42] In comparison with the materials here, a very slight low-energy absorption shoulder for TPT is observed, indicating the presence of some homocouplings. A comparison of the observed bandgap of our TPT material with the same material in this recent report by Janssen et al. suggests that a minimal amount of homocouplings (<5%) are present.[42] The observation of very slight low-energy broadening in the absorption spectra of TPfT, TTT, and TTfT suggests that there may be some homocouplings in these materials as well.

Onset of polymer oxidation was measured by CV as shown in Figure 2. The E_{HOMO} levels are reported versus an external ferrocene reference (−4.8 V from vacuum) in Figure 3. TTT and TPT display similar E_{HOMO} levels while TTfT and TPfT show reduced E_{HOMO} levels, by about 0.1−0.2 eV each. This is consistent with many previous studies that have substituted fluorine atoms along the polymer backbone. Generally, a decrease of 0.1−0.2 eV is observed depending on the electronic nature of the polymer backbone.[22,24,25,28,33] These results suggest that the fluorinated TTfT and TPfT should exhibit improved V_{oc} in OPV devices. Previous reports have shown that substitution of the alternating thiophene unit in TTT for a phenyl unit (TPT) results in a lowering of the E_{HOMO} level by >0.1 eV, while in this study a more moderate reduction of the E_{HOMO} (~0.5 eV) was observed.[5,9]

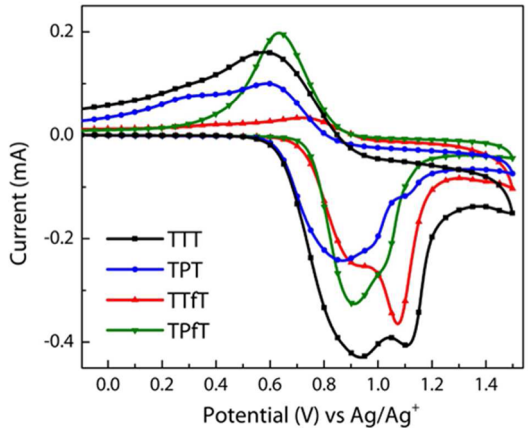

Figure 2. Cyclic voltammograms of the oxidation onsets for TTT, TPT, TTfT, and TPfT versus the Ag/Ag^+ redox potential. Measurements were performed on polymer films cast directly on the working electrode.

By combining the measured E_{HOMO} level and the onset of absorption the bandgap profile of these materials can be compared, as shown in Figure 3. Since these materials are designed to function with a PCBM type acceptor, the bandgap profile of PCBM is also shown for comparison. In this representation of the polymer bandgaps, the reduction of the E_{HOMO} level in the two fluorinated materials TTfT and TPfT can more clearly be seen. Additionally, the bandgaps for TTT and TPT closely resemble those in their fluorinated counterparts TTfT and TPfT, indicating that the fluorination does not greatly affect the absorption for these materials. Upon examination of the E_{LUMO} levels it can be seen that the lowered E_{HOMO} levels in TTfT and TPfT and the low bandgap nature of these materials results in a reduced $E_{LUMO}^{DONOR} - E_{LUMO}^{PCBM}$ offset, which can result in reduced OPV device efficiencies. Many studies suggest that a minimum E_{LUMO} offset of 0.3 eV is required for efficient charge separation.

The absorption and the observed E_{HOMO} levels of these materials are consistent with previous reports, suggesting that these materials should also perform well in both OPV and OFET applications. Thus, bulk heterojunction OPV type devices with the standard device architecture were fabricated. Each of the polymers blended with $PC_{71}BM$ were deposited on PEDOT:PSS, and then the active layers were coated with a calcium interlayer and aluminum electrode. $J-V$ curves for representative average devices are shown in Figure 4, and average device characteristics are given in Table 2. Previous examples of TTT and TPT synthesized by Suzuki coupling reached efficiencies of 4.7% and 5.5% after careful optimization

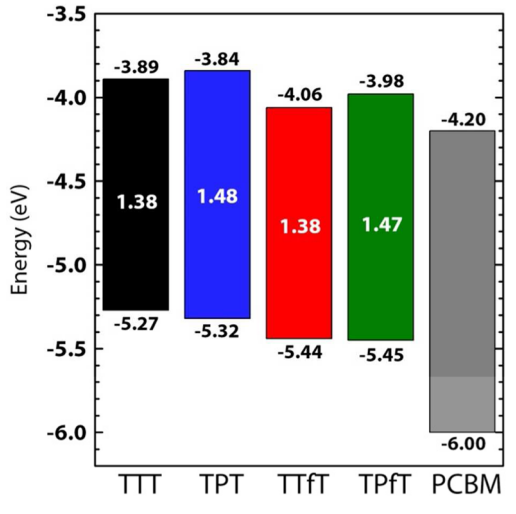

Figure 3. Polymer energy level and bandgap profiles. E_{homo} levels as measured by CV. Optical bandgap determined from UV−vis absorption onset. E_{lumo} determined as follows: $E_{lumo} = E_{homo} - E_g^{opt}$.

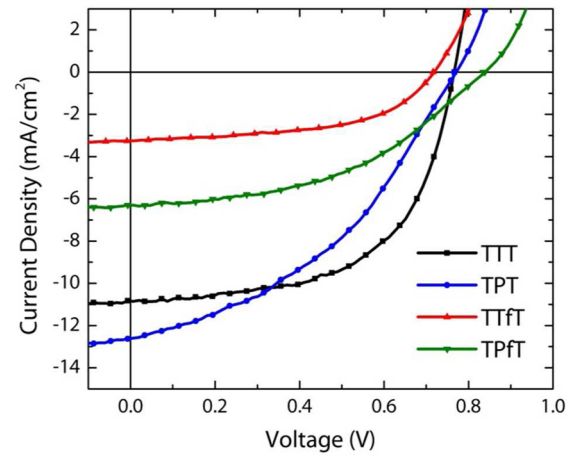

Figure 4. Current density−voltage characteristics of polymer:$PC_{71}BM$ bulk heterojunction OPV devices.

DOI: 10.1021/acs.macromol.5b01275
Macromolecules 2015, 48, 6978−6986

Table 2. Photovoltaic Characteristics of Polymer:$PC_{71}BM$ OPV Devices[a]

	V_{oc} [V]	J_{sc} [mA/cm^2]	FF	PCE [%]	PCE^{best} [%]
TTT[b]	0.70 ± 0.01	10.05 ± 0.29	54.79 ± 1.4	3.85 ± 0.13	4.01
TPT[c]	0.76 ± 0.01	12.86 ± 0.40	39.89 ± 1.6	3.91 ± 0.32	4.37
TTfT[b]	0.70 ± 0.01	3.17 ± 0.09	53.00 ± 0.70	1.17 ± 0.05	1.25
TPfT[c]	0.83 ± 0.02	6.14 ± 0.28	44.87 ± 0.57	2.29 ± 0.08	2.40

[a]Measurements represent average ± standard deviation for >6 devices. [b]Processed from CB with 3% DIO. [c]Processed from CF: DCB (4:1).

of the solvent system used for processing the thin-film active layer.[8,9]

V_{oc} values of 0.7−0.8 V were obtained for each of the materials, following the observed trends in the measured E_{HOMO} levels. TPfT shows an increase of ∼0.07 V in the V_{oc} in comparison to TPT, and TPT shows a slightly higher V_{oc} in comparison to TTT, which correlates well to the measured E_{HOMO} levels. Despite the reduced E_{HOMO} of TTfT, however, there is no increase in the V_{oc} for TTfT in comparison to TTT.

For TTT and TPT, high J_{sc} values (10−12 mA/cm^2) were obtained, as is characteristic of low bandgap polymers and DPP-based materials in general. However, J_{sc} values obtained for TTfT and TPfT were significantly lower, 3.17 mA/cm^2 and 6.14 mA/cm^2. Since these materials display similar absorption profiles to the nonfluorinated materials TTT and TPT, and good charge mobility as will be discussed later, the reduction in J_{sc} may be related to the $E_{LUMO}^{DONOR} - E_{LUMO}^{PCBM}$ energy level offset. For TTfT and TPfT, the E_{LUMO} offsets with PCBM are 0.14 and 0.22 eV, which is significantly below the 0.3 V offset threshold design criteria for most materials designed to function with PCBM. Moreover, we notice that the E_{LUMO} offset in our materials scales with the observed J_{sc}. TTfT with the lowest E_{LUMO} offset of 0.14 eV has the lowest J_{sc} of 3.17 mA/cm^2. TPfT has a slightly higher offset of 0.22 eV and slightly higher J_{sc} of 6.14 mA/cm^2. This trend can also be extended to TTT and TPT. It is well-known that the "threshold" offset of 0.3 eV promotes charge separation, reducing charge recombination within the donor material, which is likely the dominant factor in the lower observed J_{sc} in TTfT and TPfT.

To achieve optimum device performance different solvent processing conditions were required for spin coating the thin-films. The TPT and TPfT materials performed optimally when processed from a binary mixture of CF:DCB (4:1), whereas the TTT and TTfT materials performed optimally when processed from CB with 3% by volume of DIO. The morphology of DPP polymers depends heavily on the solvent used for processing. Using different solvent combinations results in the formation of a more defined fibrillar polymer morphology that allows for more efficient charge separation and transport.[8,9,43−45] This is consistent with the TEM analysis discussed below. Average device PCEs of 3.85% and 3.91% were achieved for the TTT and TPT materials. These PCEs are slightly lower compared to the maximum PCEs of 4.7% and 5.5% for TTT and TPT previously noted by Janssen et al.[8,9] Nonetheless, our results suggest that DArP can be a viable alternative to Stille and Suzuki polycondensation methods for the synthesis of high-quality conjugated polymeric materials.

TEM was used to evaluate the morphology of the polymer:PCBM bulk-heterojunction blends as shown in Figure 5. Thin films were produced in an identical manner to the optimized OPV devices. DPP is known to be a highly crystalline conjugated polymer building block which produces fibrillar type morphological features when blended with PCBM

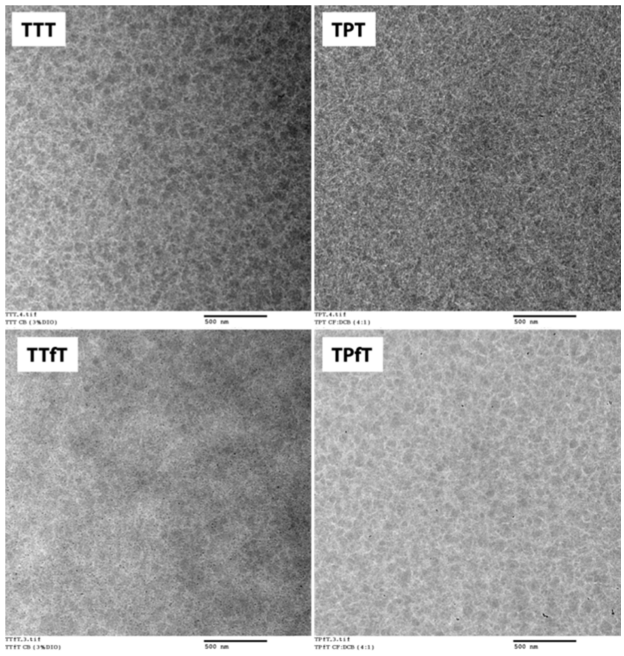

Figure 5. TEM images of polymer:PCBM films. Films were prepared identically to optimized OPV devices. Scale bar is 500 nm.

and processed from appropriate solvent systems.[43,44,46] A fibrillar network was seen for each of the different active layers. The addition of fluorine on the polymer backbone in TTfT and TPfT did not lead to the formation of large phase separated domains or enhancement of the polymer crystallinity.

Resonant soft X-ray scattering (RSoXS) of the TPT blends (Figure 6) showed a broad peak located at ∼0.008 Å^{-1}, giving a center-to-center distance of 78 nm, corresponding to the mesh-size of the fibrillar networks. Addition of the fluorine atoms into

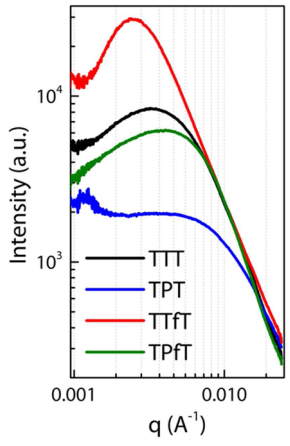

Figure 6. RSoXS profiles for polymer:PCBM blend thin films. Films were prepared identically with those for optimized OPV devices.

DOI: 10.1021/acs.macromol.5b01275
Macromolecules 2015, 48, 6978−6986

the TPT backbone led to enhanced scattering intensities with an increase in the mesh size for the TPfT material. A broad scattering peak at 0.0039 $Å^{-1}$ was seen, corresponding to a distance of 161 nm. TTT gives a stronger scattering peak at 0.0034 $Å^{-1}$, corresponding to a distance of 185 nm. The high J_{sc} observed for TTT indicates that the change from the phenyl unit (in TPT) to thiophene in the TTT backbone promotes ordering of the TTT and enhanced charge separation and collection. TTfT blends showed a much more intense scattering peak located at 0.0025 $Å^{-1}$, giving a distance of 251 nm. This spacing correlates well with expectations considering the morphology and device performance. For TTfT It should be noted that larger aggregations could be seen in the TEM images as a result of either film thickness variations or PCBM aggregations, which could be limiting in the performance of TTfT OPV devices.

It should be mentioned that TTT and TTfT devices fabricated with the CF:DCB solvent system performed poorly in comparison to those prepared from CB with 3% DIO additive. This arises from the formation of large scale phase separated domains. This is evidenced by TEM and RSoXS data shown in Figures S17 and S18. TTT and TTfT blends processed from CF:DCB show a macroscopic phase separation of polymer enriched and PCBM enriched domains, which are hundreds of nanometers in size. When processed from CB with 3% DIO, these same materials form fibrillar morphologies, as shown in Figure 5, leading to enhanced device performance. This effect has been noted in previous studies of DPP materials.

The structure order of DPP polymers in pure and blend thin films were probed by grazing incidence wide-angle X-ray diffraction (GIWAXS). 2-D GIWAXS images for both pure polymer and blend films are available in the Supporting Information (Figures S20–S29). Out-of-plane and in-plane line cuts are summarized in Figure 7. First, examining the profile from pure polymer films in the q_z direction the (100) peak at ~0.36 A^{-1} corresponds to an interchain d-spacing of 1.74 nm for each of these polymers. TTT showed relatively lower (100) intensity, while TPT showed high (100) intensity with higher order diffraction peaks, indicating a higher degree of crystallinity for this material. TPT and TTT exhibited a (010) reflection at ~1.7 A^{-1}, corresponding to a $\pi-\pi$ spacing of 3.7 Å. The fluorinated polymers showed moderate (100) intensity for both samples. More importantly, the $\pi-\pi$ stacking peak was slightly shifted to higher q region (~1.75 A^{-1}), giving a smaller distance of 3.59 Å. Thus, for TTfT and TPfT, fluorination in the backbone promotes interchain stacking. Substitution of fluorine atoms has previously been suggested to reduce steric hindrance between adjacent units, promoting greater backbone planarity and thus, a closer $\pi-\pi$ stacking.[31,34] This effect is also noticed in the OFET mobility measurements for TTfT and TPfT as will be discussed below.

GIWAXS for the polymer:PCBM blends exhibit several features that are characteristic of polymer crystallinity. First, the (100) can again be seen ~0.36 A^{-1} in both the out-of-plane and in-plane directions indicating a degree of mixed orientation. A broad reflection arising from the PCBM is seen ~1.35 A^{-1} for all the materials. The broad shoulder at ~1.7 A^{-1} is characteristic of the (010) reflection, though it is obscured by the scattering from the PCBM. This feature can be observed in both the q_z and q_{xy}, indicative of mixed edge-on and face-on orientation of the crystals. Analysis of the relative intensity of the (010) peaks in the q_z and q_{xy} does not indicate any increase or decrease of face-on orientation in the fluorinated TTfT and TPfT materials.

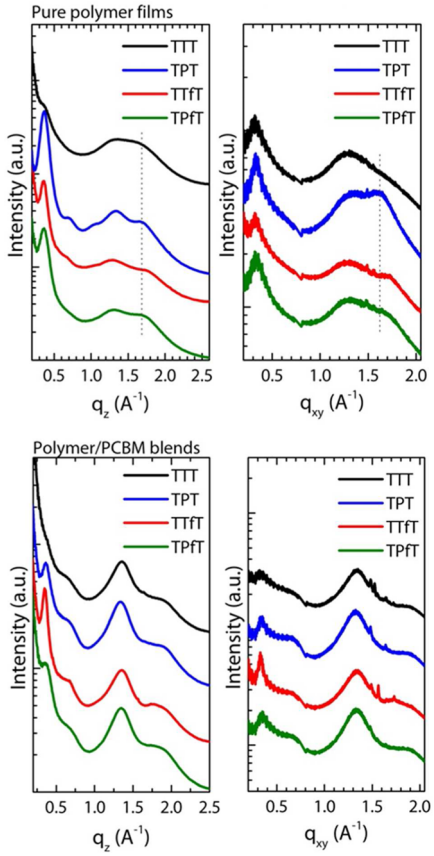

Figure 7. GIWAXS out-of-plane q_z (left) and in-plane q_{xy} (right) measurements for pure polymer thin films (top) and polymer:PCBM blend thin films (bottom).

In addition to OPV devices, these materials were also evaluated for use in OFET applications. Bottom-gate, bottom-contact configuration OFETs were fabricated with an n-doped silicon gate and a silicon dioxide dielectric and were characterized under ambient conditions. Output and transfer curves, as well as mobility characteristics for each of the materials are shown in Figures 8 and 9, respectively. Each of the four polymers showed excellent hole transport properties, on the order of 0.01–0.06 $cm^2\ V^{-1}\ s^{-1}$. Interestingly, the fluorinated materials TTfT and TPfT exhibited increased hole mobility, approximately 2–3 times greater than their corresponding nonfluorinated materials TTT and TPT. This significant improvement stems, more than likely, from the more planar polymer backbone confirmation due to the fluorine functionalization, which allows for slightly closer $\pi-\pi$ stacking as evidenced by the GIWAXS data. As shown in Figure 9, the fluorinated materials TTfT and TPfT also showed air-stable electron transport. This is a result of the lower E_{LUMO} compared to the nonfluorinated TTT and TPT. Thus, these OFET measurements again demonstrate that the materials synthesized by DArP can produce high mobility materials, and that fluorination can be an effective tool for enhancing both hole and electron mobility.

3.0. CONCLUSION

The successful synthesis of a series of DPP-based polymers using DArP methodologies has been documented. Four

DOI: 10.1021/acs.macromol.5b01275
Macromolecules 2015, 48, 6978–6986

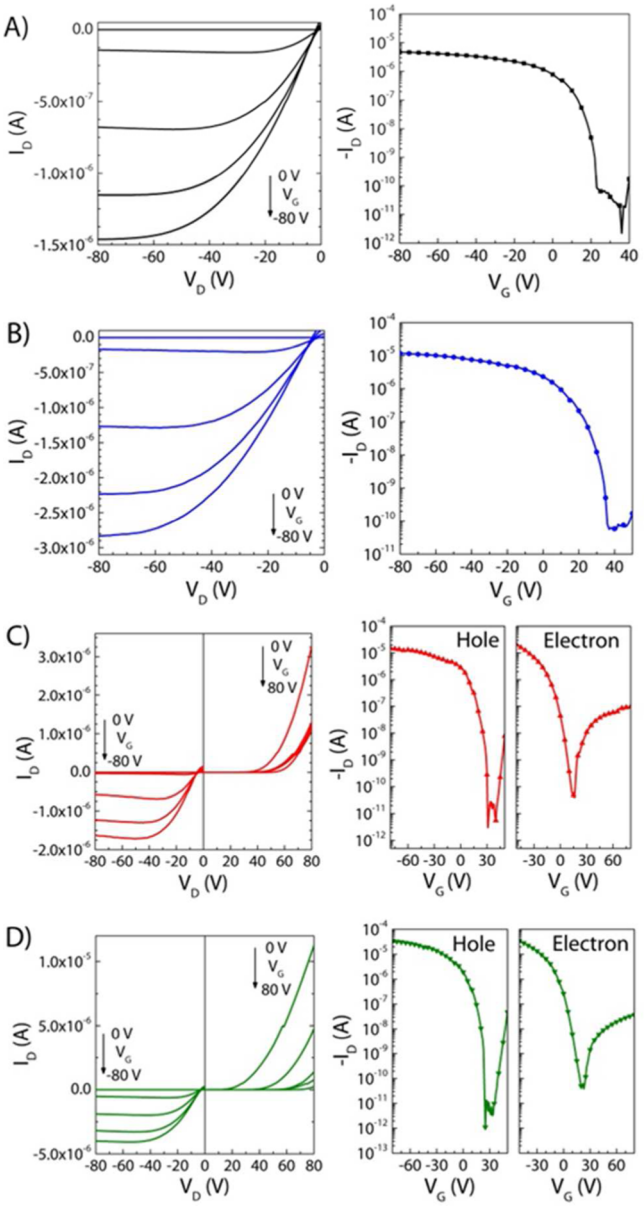

Figure 8. Current−voltage characteristics of OFETs. Output (left column) and transport (right column) characteristics are shown for (A) TTT, (B) TPT, (C) TTfT, and (D) TPfT. In the transfer curves, V_{DS} = −80 V for hole transport and V_{DS} = 80 V for electron transport. No N-channel property was found in TTT- and TPT-based devices.

polymer materials TTT, TPT, TTfT and TPfT were synthesized and the structure−property-performance relationships were studied. These polymers were found to be high molecular weight, ranging from 10 to 30 kg/mol M_n, 17−110 kg/mol M_w. The repeating nature of each of the polymer structures was verified by NMR and MALDI−TOF mass spectroscopy. Additionally, characterization of the absorbance and onset of oxidation have shown that the polymers synthesized by DArP have optical and electrical properties similar to those previously synthesized by Stille or Suzuki polycondensation methods. This suggests that DArP may be a practical synthetic alternative. In the TTfT and TPfT materials, the effect of fluorine substitution on the polymer backbone was shown to significantly reduce the E_{homo} (by 0.1−0.2 eV), promote closer $\pi-\pi$ stacking of the polymer chains, while

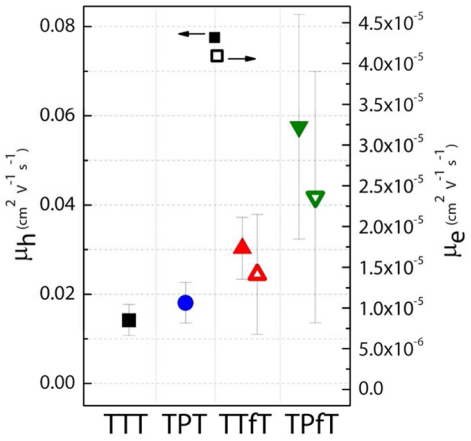

Figure 9. OFET hole (μ_h) and electron (μ_e) mobilities measured in air. Measurements are averaged over five devices with the error bars representing the standard deviation.

maintaining similar absorption profiles to the nonfluorinated comparisons TTT and TPT. Each of the four materials formed distributed, fibrillar-like bulk heterojunction blends when mixed with PCBM as verified by TEM. OPV and OFET devices were fabricated to test the performance of these materials. In OPVs, average device efficiencies of 3.8−3.9% were achieved for our TTT and TPT materials, which is also comparable to previously reported data for TTT and TPT materials synthesized by Stille and Suzuki polycondensation. For TTfT and TPfT, OPV efficiencies were much lower due to an insufficient energy separation between the $E_{LUMO}^{Polymer}$ and E_{LUMO}^{PCBM}. Also, slightly larger domain spacings were observed in the fluorinated materials, which often leads to greater charge recombination and inefficient charge separation and resulting in lower J_{sc}. In OFETs, each of the four materials exhibited high hole-mobilities on the order of 10^{-2} $cm^2V^{-1}s^{-1}$. The fluorinated TTfT and TPfT displayed enhanced hole-mobilites, by 2−3×. Because of their lower E_{LUMO}, TTfT and TPfT also exhibited air-stable electron transport properties. The performance of these materials has demonstrated that DArP can be an effective tool for conjugated polymer synthesis, producing quality materials that perform well in organic electronic applications. Moreover, the effectiveness of fluorine substitution for tuning the electronic properties of conjugated polymers has been demonstrated, which can be used to enhance device performance when applied correctly.

4.0. EXPERIMENTAL SECTION

4.1. Materials. All reagents and chemicals were purchased from commercial sources (Matrix Scientific, Sigma-Aldrich, Acros Organics, Alfa Aesar) and used without further purification unless stated otherwise. The (2-hexyl)decyl substituted DPP core unit was synthesized in a similar manner to previous reports.[36] **M3** (2,5-dibromo-3,4-difluorothiophene) was synthesized as reported.[37] All reactions were performed under inert (N_2) atmosphere.

4.2. Characterization. ^1H and ^{19}F NMR spectra were collected with a 500 MHz Agilent Technologies instrument with variable temperature capability. UV−vis absorption measurements of polymer solutions and films were performed on a PerkinElmer Lamba 25 UV−vis spectrometer. Solution spectra were measured from dilute polymer solutions in $CHCl_3$ at RT. Films for absorption spectra were spin-coated from 10 mg/mL polymer solutions in $CHCl_3$ at 1500 rpm for 60 s. Polymer molecular weight and dispersity ($Đ$) analysis was completed via gel-permeation chromatography (GPC) in 1,2,4-trichlorobenzene at 135 °C using a Polymer Laboratories PL-220

DOI: 10.1021/acs.macromol.5b01275
Macromolecules 2015, 48, 6978−6986

high- temperature GPC instrument calibrated against polystyrene standards. MALDI−TOF experiments were performed on a Bruker microflex instrument, using either terthiophene or DCTB (*trans*-2-[3-(4-*tert*-butylphenyl)-2-methyl-2-propenylidene]malononitrile) as the ionizing matrix (1:1000 w/w polymer to matrix). Cyclic voltammetry (CV) measurements of the polymer films were done with a Bioanalytical Systems Inc. (BASi) EC Epsilon potentiostat using a three-electrode configuration consisting of a glassy carbon working electrode, a $Ag/AgNO_3$ (0.01 M in acetonitrile) reference electrode, and a Pt wire counter electrode in tetrabutylammonium hexafluorophosphate electrolyte solution (0.1 M) in acetonitrile. Measurements were calibrated to the ferrocene/ferrocenium redox couple (Fc/Fc^+) external reference. Films for CV were drop-cast directly onto the glassy carbon working electrode from polymer solutions in $CHCl_3$. Bright-field TEM was conducted using a JEOL 2000 FX TEM instrument operating at an accelerating voltage of 200 kV. Active layer films for TEM were spin-coated in the same manner as for OPV devices on PEDOT:PSS. The films were then floated onto copper TEM grids in water.

4.3. Typical Polymerization Procedure. All polymers were synthesized using the same optimized DArP procedure. A typical polymerization procedure was completed as described. Into a 20 mL reaction vial with septa was added 0.5 mmol DPP core (374.6 mg), 0.5 mmol **M1**−**M4**, 15.5 mg $Pd_2dba_3CHCl_3$ (3 mol %), 21.1 mg of P(*o*-MePh)$_3$ (12 mol %), 51.1 mg of PivOH (1 equiv), and 488.7 mg of Cs_2CO_3 (3 equiv). The vial was then sealed and purged with N_2 for 20 m. Toluene:DMF (10:1 v/v, 11 mL, 0.05 M) was then added as solvent and the mixture degassed with N_2 for 20 m. The reaction mixture was stirred at room temperature for 20 m then heated to 115 °C for 20 h. After completion of the reaction time, the contents of the reaction vessel were then cooled and precipitated into stirring methanol. $CHCl_3$ was used to dissolve any solid material prior to precipitation. All precipitated solids were then collected by filtration and subjected to sequential Soxhlet extraction with methanol, acetone, hexanes, and $CHCl_3$. Polymers were then precipitated from $CHCl_3$ and subjected to one more round of Soxhlet extraction following the same sequential procedure. The $CHCl_3$-extracted materials were then used for the remainder of the polymer characterization.

4.4. OPV Device Preparation. Standard device architecture (ITO/PEDOT:PSS/active layer/Ca/Al) was used. Indium tin oxide (ITO) coated glass substrates (20 ± 5 ohms/square) were purchased from Thin Film Devices Inc. Substrates were cleaned through ultrasonic treatment in detergent, water (2×), acetone, and isopropyl alcohol and dried in an oven overnight. The ITO substrates were then cleaned by ultraviolet ozone treatment (15 min) and PEDOT:PSS (Clevios P VP A1 4083) was spin-coated in air (3500 rpm, 40 s) forming ∼35 nm films. After annealing the PEDOT:PSS at 150 °C for 30 min in air, the substrates were transferred into a glovebox under inert atmosphere. Polymer/$PC_{71}BM$ (1:2 w/w) solutions were then spin-coated on top of the PEDOT:PSS layer at 2000 rpm for 60 s. The thickness of the active layer polymer/$PC_{71}BM$ films were ∼80−100 nm (KLA-TENCOR Alpha-Step IQ Surface Profiler). Finally, 15 nm of calcium and 100 nm of aluminum were thermally evaporated on the active layer under high vacuum (2×10^{-4} Pa) to complete the devices. The areas of the devices were 6 mm^2, as defined by the evaporator shadow mask area. Current−voltage (J−V) characteristics of the devices were measured under simulated AM1.5G irradiation (100 mW cm^{-2}) using a Xe lamp-based Newport 91160 300-W solar simulator. The light intensity was adjusted with an NREL-calibrated Si solar cell with a KG-5 filter. Device characteristics are reported as an average of at least six devices ± the standard deviation of those measurements.

4.5. OFET Device Fabrication. Organic field effect transistors (OFETs) were fabricated in a bottom gate, bottom contact configuration. Highly *n*-doped silicon and thermally grown silicon dioxide (300 nm) were used as the back gate and gate dielectric, respectively. Source and drain electrodes (5 nm Cr/45 nm Au), having a channel width (W = 140 μm)/channel length (L = 5 μm) = 28, were prepared using standard photolithographic procedures. The substrates were then cleaned with pure water, hot concentrated sulfuric acid/hydrogen peroxide solution (2:1 v/v), water, and then isopropyl alcohol. Then vaporized trichloro(octadecyl)silane (OTS) was used for the surface modification of the gate dielectric layer. The characterization was completed using a Keithley 4200 SCS probe station under ambient atmosphere. Then field effect mobilities were calculated using the standard equation for the saturation region in metal-dioxide-semiconductor field effect transistors: $I_d = \mu(W/2L)C_i(V_g - V_t)^2$, where I_d is drain-source current, μ is field effect mobility, W and L are the channel width and length, C_i is the capacitance per unit area of the gate insulator (C_i = 10 nF/cm^2), V_g is the gate voltage and V_t is the threshold voltage. OFET mobilities are reported as an average of five devices ± the standard deviation of those measurements.

4.6. GIWAXS Measurements. Grazing incidence wide-angle X-ray scattering (GIWAXS) characterization of active layer was performed at beamline 7.3.3, Advanced Light Source (ALS), Lawrence Berkeley National Lab (LBNL). X-ray energy was 10 keV and operated in top off mode. The scattering intensity was recorded on a 2 D image plate (Pilatus 2M) with a pixel size of 172 μm (1475 × 1679 pixels). The samples were ∼15 mm long in the direction of the beam path, and the detector was located at a distance of 300 mm from the sample center (distance calibrated by AgB reference). The incidence angle was chosen to be 0.16° to optimize the signal-to-background ratio. Thin-film samples were prepared on PEDOT:PSS covered Si wafers in a similar manner to the OPV devices and pure polymer samples were prepared on Si wafers with a 2 nm natural oxide layer.

4.7. RSoXS Measurements. Resonant Soft X-ray Scattering experiments were carried out in beamline 11.0.1.2, ALS, LBNL. Experiments were done in transmission geometry. BHJ thin films were flowed in water and transferred onto Silicon Nitride windows from Norcada Inc. Samples were loaded into a high vacuum chamber (∼10^{-7} Torr) to avoid carbon contaminations in ambient environment. A phonton energy of 284.2 eV was used in runing the experiments, which gave best contrast at carbon K-edge. 300 nm polystyrene spheres were used as standard to calibrate sample-to-detecter distance. Recorded data were processed using beamline developed macros that were embeded in the Igor software package.

■ ASSOCIATED CONTENT

Ⓢ Supporting Information

The Supporting Information is available free of charge on the ACS Publications website at DOI: 10.1021/acs.macromol.5b01275.

Table of GPC molecular weights and figures showing MALDI−TOF mass spectra, ^1H and ^{19}F NMR spectra, TEM images, RSoXS profiles, GIWAXS line scans, GIWAXS 2-D images, and GPC traces (PDF)

■ AUTHOR INFORMATION

Corresponding Authors

*(E.B.C.) E-mail: Coughlin@mail.pse.umass.edu.
*(T.P.R.) E-mail: Russell@mail.pse.umass.edu.

Notes

The authors declare no competing financial interest.

■ ACKNOWLEDGMENTS

This work is supported as part of Polymer-Based Materials for Harvesting Solar Energy (PHaSE), an Energy Frontier Research Center funded by the U.S. Department of Energy, Office of Science, Office of Basic Energy Sciences under Award Number DE-SC0001087. Portions of this research were carried out at the Advanced Light Source and Molecular Foundry, Berkeley National Laboratory, which is supported by the DOE, Office of Science, and Office of Basic Energy Sciences.

DOI: 10.1021/acs.macromol.5b01275
Macromolecules 2015, 48, 6978−6986

REFERENCES

(1) Bronstein, H.; Chen, Z.; Ashraf, R. S.; Zhang, W.; Du, J.; Durrant, J. R.; Shakya Tuladhar, P.; Song, K.; Watkins, S. E.; Geerts, Y.; Wienk, M. M.; Janssen, R. a J.; Anthopoulos, T.; Sirringhaus, H.; Heeney, M.; McCulloch, I. *J. Am. Chem. Soc.* **2011**, *133*, 3272−3275.
(2) Qu, S.; Tian, H. *Chem. Commun.* **2012**, *48*, 3039.
(3) Nielsen, C. B.; Turbiez, M.; McCulloch, I. *Adv. Mater.* **2013**, *25*, 1859−1880.
(4) Dou, L.; You, J.; Yang, J.; Chen, C.; He, Y.; Murase, S.; Moriarty, T.; Emery, K.; Li, G.; Yang, Y. *Nat. Photonics* **2012**, *6*, 180−185.
(5) Hendriks, K. H.; Heintges, G. H. L.; Gevaerts, V. S.; Wienk, M. M.; Janssen, R. A. J. *Angew. Chem., Int. Ed.* **2013**, *52*, 8341−8344.
(6) Li, W.; Furlan, A.; Hendriks, K. H.; Wienk, M. M.; Janssen, R. a J. *J. Am. Chem. Soc.* **2013**, *135*, 5529−5532.
(7) Zambounis, J. S.; Hao, Z.; Iqbal, A. *Nature* **1997**, *388*, 131.
(8) Bijleveld, J. C.; Zoombelt, A. P.; Mathijssen, S. G. J.; Wienk, M. M.; Turbiez, M.; de Leeuw, D. M.; Janssen, R. A. J. *J. Am. Chem. Soc.* **2009**, *131*, 16616−16617.
(9) Bijleveld, J. C.; Gevaerts, V. S.; Di Nuzzo, D.; Turbiez, M.; Mathijssen, S. G. J.; de Leeuw, D. M.; Wienk, M. M.; Janssen, R. a J. *Adv. Mater.* **2010**, *22*, E242−E246.
(10) Mercier, L. G.; Leclerc, M. *Acc. Chem. Res.* **2013**, *46*, 1597−1605.
(11) Okamoto, K.; Zhang, J.; Housekeeper, J. B.; Marder, S. R.; Luscombe, C. K. *Macromolecules* **2013**, *46*, 8059−8078.
(12) Facchetti, A.; Vaccaro, L.; Marrocchi, A. *Angew. Chem., Int. Ed.* **2012**, *51*, 3520−3523.
(13) Wang, K.; Wang, M. *Curr. Org. Chem.* **2013**, *17*, 999−1012.
(14) Pouliot, J.-R.; Sun, B.; Leduc, M.; Najari, A.; Li, Y.; Leclerc, M. *Polym. Chem.* **2015**, *6*, 278−282.
(15) Sonar, P.; Foong, T. R. B.; Dodabalapur, A. *Phys. Chem. Chem. Phys.* **2014**, *16*, 4275−4283.
(16) Liu, S.-Y.; Fu, W.-F.; Xu, J.-Q.; Fan, C.-C.; Jiang, H.; Shi, M.; Li, H.-Y.; Chen, J.-W.; Cao, Y.; Chen, H.-Z. *Nanotechnology* **2014**, *25*, 014006.
(17) Liu, S. Y.; Liu, W. Q.; Xu, J. Q.; Fan, C. C.; Fu, W. F.; Ling, J.; Wu, J. Y.; Shi, M. M.; Jen, A. K. Y.; Chen, H. Z. *ACS Appl. Mater. Interfaces* **2014**, *6*, 6765−6775.
(18) Hendsbee, A. D.; Sun, J.-P.; Rutledge, L. R.; Hill, I. G.; Welch, G. C. *J. Mater. Chem. A* **2014**, *2*, 4198.
(19) Guo, Q.; Dong, J.; Wan, D.; Wu, D.; You, J. *Macromol. Rapid Commun.* **2013**, *34*, 522−527.
(20) Liu, S.-Y.; Shi, M.-M.; Huang, J.-C.; Jin, Z.-N.; Hu, X.-L.; Pan, J.-Y.; Li, H.-Y.; Jen, A. K.-Y.; Chen, H.-Z. *J. Mater. Chem. A* **2013**, *1*, 2795.
(21) Morin, P.; Bura, T.; Sun, B.; Gorelsky, S. I.; Li, Y.; Leclerc, M. *ACS Macro Lett.* **2015**, *4*, 21−24.
(22) Zhang, M.; Guo, X.; Zhang, S.; Hou, J. *Adv. Mater.* **2014**, *26*, 1118−1123.
(23) Chen, H.-C.; Chen, Y.-H.; Liu, C.-C.; Chien, Y.-C.; Chou, S.-W.; Chou, P.-T. *Chem. Mater.* **2012**, *24*, 4766−4772.
(24) Albrecht, S.; Janietz, S.; Schindler, W.; Frisch, J.; Kurpiers, J.; Kniepert, J.; Inal, S.; Pingel, P.; Fostiropoulos, K.; Koch, N.; Neher, D. *J. Am. Chem. Soc.* **2012**, *134*, 14932−14944.
(25) Zhou, H.; Yang, L.; Stuart, A. C.; Price, S. C.; Liu, S.; You, W. *Angew. Chem., Int. Ed.* **2011**, *50*, 2995−2998.
(26) Price, S. C.; Stuart, A. C.; Yang, L.; Zhou, H.; You, W. *J. Am. Chem. Soc.* **2011**, *133*, 4625−4631.
(27) Liang, Y.; Xu, Z.; Xia, J.; Tsai, S.-T.; Wu, Y.; Li, G.; Ray, C.; Yu, L. *Adv. Mater.* **2010**, *22*, E135−E138.
(28) Liang, Y.; Feng, D.; Wu, Y.; Tsai, S.; Li, G.; Ray, C.; Yu, L. *J. Am. Chem. Soc.* **2009**, *131*, 7792−7799.
(29) Liu, P.; Zhang, K.; Liu, F.; Jin, Y.; Liu, S.; Russell, T. P.; Yip, H.; Huang, F.; Cao, Y. *Chem. Mater.* **2014**, *26*, 3009.
(30) Homyak, P. D.; Liu, Y.; Ferdous, S.; Liu, F.; Russell, T. P.; Coughlin, E. B. *Chem. Mater.* **2015**, *27*, 443−449.
(31) Bronstein, H.; Frost, J. M.; Hadipour, A.; Kim, Y.; Nielsen, C. B.; Ashraf, R. S.; Rand, B. P.; Watkins, S.; McCulloch, I. *Chem. Mater.* **2013**, *25*, 277−285.
(32) Yang, L.; Tumbleston, J. R.; Zhou, H.; Ade, H.; You, W. *Energy Environ. Sci.* **2013**, *6*, 316−326.
(33) Son, H. J.; Wang, W.; Xu, T.; Liang, Y.; Wu, Y.; Li, G.; Yu, L. *J. Am. Chem. Soc.* **2011**, *133*, 1885−1894.
(34) Park, J. H.; Jung, E. H.; Jung, J. W.; Jo, W. H. *Adv. Mater.* **2013**, *25*, 2583−2588.
(35) Park, S.; Cho, J.; Ko, M. J.; Chung, D. S.; Son, H. J. *Macromolecules* **2015**, *48*, 3883.
(36) Huo, L.; Hou, J.; Chen, H.-Y.; Zhang, S.; Jiang, Y.; Chen, T. L.; Yang, Y. *Macromolecules* **2009**, *42*, 6564−6571.
(37) Sakamoto, Y.; Komatsu, S.; Suzuki, T. *J. Am. Chem. Soc.* **2001**, *123*, 4643−4644.
(38) Wakioka, M.; Kitano, Y.; Ozawa, F. *Macromolecules* **2013**, *46*, 370−374.
(39) Homyak, P. D.; Tinkham, J.; Lahti, P. M.; Coughlin, E. B. *Macromolecules* **2013**, *46*, 8873−8881.
(40) Matthews, J. R.; Niu, W.; Tandia, A.; Wallace, A. L.; Hu, J.; Lee, W.-Y.; Giri, G.; Mannsfeld, S. C. B.; Xie, Y.; Cai, S.; Fong, H. H.; Bao, Z.; He, M. *Chem. Mater.* **2013**, *25*, 782−789.
(41) De Winter, J.; Deshayes, G.; Boon, F.; Coulembier, O.; Dubois, P.; Gerbaux, P. *J. Mass Spectrom.* **2011**, *46*, 237−246.
(42) Hendriks, K. H.; Li, W.; Heintges, G. H. L.; Van Pruissen, G. W. P.; Wienk, M. M.; Janssen, R. a J. *J. Am. Chem. Soc.* **2014**, *136*, 11128−11133.
(43) Liu, F.; Gu, Y.; Wang, C.; Zhao, W.; Chen, D.; Briseno, A. L.; Russell, T. P. *Adv. Mater.* **2012**, *24*, 3947−3951.
(44) Ye, L.; Zhang, S.; Ma, W.; Fan, B.; Guo, X.; Huang, Y.; Ade, H.; Hou, J. *Adv. Mater.* **2012**, *24*, 6335−6341.
(45) Liu, Y.; Liu, F.; Wang, H.; Nordlund, D.; Sun, Z.; Ferdous, S.; Russell, T. P. *ACS Appl. Mater. Interfaces* **2015**, *7*, 653−661.
(46) Ferdous, S.; Liu, F.; Wang, D.; Russell, T. P. *Adv. Energy Mater.* **2014**, *4*, 1300834.

DOI: 10.1021/acs.macromol.5b01275
Macromolecules 2015, 48, 6978−6986